

AB INITIO STABILITY INVESTIGATION OF IONIC CLATHRATE HYDRATES

Travis B. Peery* and Lawrence R. Pratt
 Los Alamos National Laboratory
 Los Alamos, NM 87545
 LA-UR-05-3237

ABSTRACT

We performed *ab initio* structural optimization simulations on two nearly identical ionic clathrate hydrates in order to identify the molecular mechanisms responsible for their large melting temperature difference. The melting temperature T_m of the β phase of *tetramethylammonium hydroxide* (TMA) clathrate $\text{Me}_4\text{NOH} \cdot 7.5\text{H}_2\text{O}$, when modified by addition of Cs^+ ions into its small polyhedral cages to form its alkali metal analog $\text{Cs}(\text{Me}_4\text{N})_2(\text{OH})_3 \cdot 14\text{H}_2\text{O}$, increases by roughly 53°C . Our DFT simulations indicate that the OH^- ions are incorporated into the water framework and that the hydroxide proton does not effectively hydrogen bond; three-fold coordinate OH^- moieties in a 4-coordinate polyhedral lattice then create a proton (hydrogen bond) deficiency. None of the relaxed clathrate configurations appeared stable in the initial tetragonal space group, with all heavy atoms shifting well outside their equivalent harmonic displacements. Besides a widely expanded distribution of $\text{O} \cdots \text{O} \cdots \text{O}$ angles in the relaxed unit cells, numerous cage edges with $r_{\text{OO}} \geq 3.25 \text{ \AA}$ were found, only $\sim 35\%$ of which corresponded to the long $(\text{O}^*-\text{H}) \cdots \text{O}$ distances through weakly interacting hydroxide protons, in direct contrast to the X-ray data. Addition of the Cs^+ ions shortened the $(\text{O}^*-\text{H}) \cdots \text{O}$ distances by $\sim 0.2 \text{ \AA}$, but left the remaining $\text{O}^* \cdots \text{O}$ distances unaffected. The hydroxide anions, while more dispersed throughout the framework than inferred from the X-ray data, were not randomly situated in the framework with respect to the cationic guests. The open, proton deficient framework of these optimized clathrates is similar to the low temperature, semiclathrate phase of TMA, suggesting a link between clathrate stability and high proton mobility along with fast orientational water dynamics. Proton ordering effects will be addressed in future work.

Keywords: ionic clathrate, ab initio molecular dynamics, density functional theory

NOMENCLATURE

r_{AB}	Distance between atom A and B
$\langle a \rangle$	Average of data 'a'
δ	Equivalent vibrational amplitude [\AA]
δE	Energy difference between Opt. and Reopt. lattices [eV]
Δr	Relaxation shift arising from optimization: $ \bar{r}_{\text{opt}} - \bar{r}_{\text{init}} $ [\AA]
$4^2 5^8$	Polyhedral 'd' cage: 2 square & 8 pentagonal faces
$5^{12} 6^3$	Polyhedral 'P' cage: 12 pentagonal & 3 hexagonal faces
$(4)^1 5^9 (5)^1 6^4 (6)^1$	Improper 16-hedron with 2 open edges & 3 open faces
Ai	Crystallographically distinct atom Ai
B	Isotropic thermal parameter [\AA^2]
$n_i^{m_i}$	Polyhedron with m_i faces of type i , each with n_i edges
$(n_i)^{m_i}$	Improper polyhedron with m_i open faces, each with n_i edges
O^*	Hydroxide oxygen
O'	O^* coordinating proton acceptor oxygen
$\text{O}^i, i \in \{1, 2, 3\}$	O^* coordinating proton donor oxygen

*Phone: (505) 667-0258, E-mail: tpeery@lanl.gov

$4^2 5^6 (5)^2 6^3$

$4^2 (4)^1 5^5 (5)$

INTRODU

Pure gas hydrates are stable under relatively low temperatures. Yet many hydrates are not well understood and guest-host interactions are important, but so are the frameworks and are less understood. Finding stable hydrates to particular applications thus requires a molecular mechanism. *Ionic* clathrate hydrates are built from a guest molecule in a unique template. *Tetramethylammonium* forms as many phases Me_4N and $n = 2(\alpha, \text{Mootz and St. of the } \beta \text{ phase by the additional changes from corresponds to eV, the structure X-ray analysis: } \text{Cs}(\text{Me}_4\text{N})_2(\text{O} \text{ group and various alkali free clathrate laboratory mechanisms in nature increase. While natural salts or other hydrates have been studied extensively, especially hydrates contribute to their$

¹Semiclathrate hydrogen-bonded

$4^25^6(5)^26^3(6)^2$	Improper 15-hedron with 3 open edges & 4 open faces
$4^2(4)^15^5(5)^1$	Improper 9-hedron with 1 open edge & 2 open faces

INTRODUCTION

Pure gas hydrates of technological interest are not stable under ambient conditions, dictating the need for relatively 'unobtrusive' phase stabilizing additives. Yet mixed (or natural) clathrate hydrates are not well understood on a molecular level. Clearly guest-host and guest-guest interactions are important, but so are guest size and geometry since host frameworks only form in the presence of guests and are less dense than even normal (Ih or Ic) ice. Finding stabilizing agents that are complementary to particular structure-controlling guests of technological interest without reducing storage capacity thus requires a clear identification of the relevant molecular mechanisms crucial to ambient stability. Ionic clathrates and semiclathrates,¹ whose frameworks are built not only of water molecules but also of a guest molecule's hydrophilic groups, represent unique templates for exploring such mechanisms in mixed clathrates.

Tetramethylammonium hydroxide $(\text{CH}_3)_4\text{N} \cdot \text{OH}$ forms as many as 8 crystalline hydrate (TMA) phases $\text{Me}_4\text{NOH} \cdot n\text{H}_2\text{O}$, where $\text{Me} \equiv (\text{CH}_3)$ and $n = 2(\alpha, \beta), 4, 5(\alpha, \beta), 7.5(\alpha, \beta)$, and 10 [1]. Mootz and Stäben [2] found that the melting point of the β phase $\text{Me}_4\text{NOH} \cdot 7.5\text{H}_2\text{O}$, when modified by the addition of Cs^+ ions into the small cages, changes from 4°C to 57°C ! While this 53°C shift corresponds to only $0.1 \text{ kcal mol}^{-1}$ or $\sim 0.45 \times 10^{-2} \text{ eV}$, the structural changes may not be small. An X-ray analysis [2] of the alkali modified clathrate $\text{Cs}(\text{Me}_4\text{N})_2(\text{OH})_3 \cdot 14\text{H}_2\text{O}$ found the same space group and very similar unit cell dimensions as the alkali free clathrate, making these systems an efficient laboratory for examining the subtle molecular mechanisms involved in the large melting temperature increase.

While natural clathrate environments often contain salts or other impurities, ionic clathrates have not been studied extensively. Exactly how ionic moieties, especially anionic or polar groups, can contribute to thermodynamic stability is not yet clear.

¹'Semiclathrates' are distinguished by open or not fully hydrogen-bonded cages.

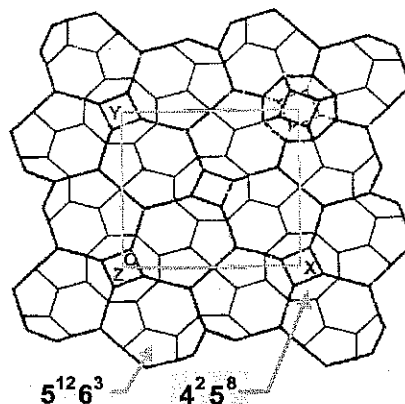


Figure 1: Unit cell schematic [2] of the TMA and Cs-TMA clathrates, consisting of 8 large $5^{12}6^3$ (P) and 4 small 4^25^8 (d) cages.

The role of hydroxide ions OH^- and proton mobility within the TMA clathrates are particularly interesting. Initial work has focused upon structural stability issues. In order to properly treat the resulting chemistry, we performed *ab initio* structural optimizations and limited molecular dynamics (AIMD) simulations of the TMA and Cs-TMA systems. Long AIMD simulations are difficult due to the large system sizes (e.g. 332 atoms).

IONIC CLATHRATES

Our initial clathrate lattices were derived from the Cs-TMA refined X-ray data of Mootz and Stäben [2], presumably equivalent to the high-temperature $7.5\text{-}\beta$ phase of the TMA clathrate.² Both thus have tetragonal unit cells, with dimensions of $a = 15.242(8)\text{\AA}$ and $c = 11.819(6)\text{\AA}$ at -50°C in space group $I4/mcm$, each containing 4 small (d) and 8 large (P) polyhedral cages: see Figs. 1 and 2. The unit cell is isostructural with the tetragonal TS-II structure, whose ideal unit cell is formed by 68 water molecules with unit cell formula $4d \cdot 8P \cdot 68\text{H}_2\text{O}$. The cationic guests and charge neutrality, however, mean that hydroxide ions replace water molecules within the host lattice, modifying the ideal unit cell formulae for TMA and Cs-TMA clathrates such that we obtain $8\text{Me}_4\text{N}(\text{OH}) \cdot 60\text{H}_2\text{O}$

²References [1] and [2] found slightly different data for the $7.5\text{-}\beta$ phase of TMA.

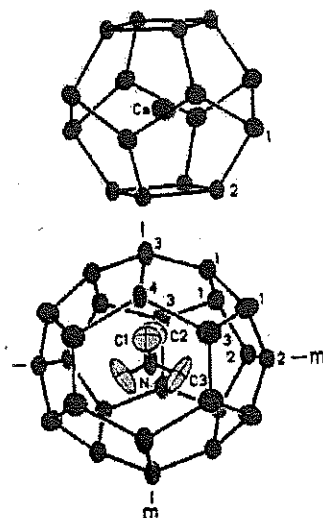


Figure 2: The small $4^2 5^8$ (above) and large $5^{12} 6^3$ (below) cages, shown with guests [2]. Crystallographically distinct sites are numbered: O1, O2, O3, and O4 (red) oxygen sites, along with the C1, C2, C3 (grey) carbon sites; mirror axes m are also shown.

and $4\text{Cs} \cdot (\text{Me}_4\text{N})_2(\text{OH})_3 \cdot 56\text{H}_2\text{O}$, respectively.

Four crystallographically distinct oxygen positions in sets of 32, 16, 16, and 16 designated as O1, O2, O3, and O4 occur, along with 3 crystallographically distinct carbon sites in sets of 16, 16, and 32 designated C1, C2, and C3.

With the addition of the Cs^+ ions into the small cages, a 2-fold orientational disorder of the Me_4N^+ ion is introduced. This Me_4N^+ disorder is coupled through a short distance of $2.27(5)$ Å between the C1 and O4 atoms, with the latter then showing a 4-fold positional disorder. This means the occupancy for the O4 and C1–C3 positions is only 25% and 50% respectively. Figure 2 shows the d and P cages with their crystallographically distinct sites labeled.

Both TMA and Cs-TMA clathrates are proton deficient, consisting of 136 cage edges and only 128 and 124 protons, respectively. According to Mootz [1], the β form of the TMA hydrate exists in a small temperature range only, close to the melting point ($4 - 6^\circ \text{C}$), suggesting that the framework is stabilized by a *dynamical* disorder above some critical value. In the corresponding low temperature α forms, the OH^- disorder may not be high enough for the pro-

ton deficiency to be compensated for. Missing protons between neighboring oxygen atoms constitutes a Bjerrum L defect³ [3], and we would expect the r_{OO} distance to increase. This, in part, leads Mootz to conclude that the largest O_i–O_i distances derived from the X-ray data correspond to hydroxide bonds. In the closed $\beta\text{-Me}_4\text{NOH} \cdot 7.5\text{H}_2\text{O}$ clathrate, this corresponds to the 16 O3–O4 distances of 3.19 Å and the 8 O3–O3 distances of 3.25 Å, over which the 8 OH^- along with 12 water molecules are supposed to be dynamically distributed; the OH^- would then be located in the P cage only.

The other reason that Mootz interpreted these O3 and O4 positions as OH^- sites relates to the hydroxide coordination he found in the $\text{Me}_4\text{NOH} \cdot 4\text{H}_2\text{O}$ hydrate, wherein one hydrogen bond length (through the hydroxide proton H^+) was ≈ 3.1 Å, *i.e.* close to the O3–O3 and O3–O4 values of the $7.5\text{-}\beta$ phase above. Interestingly, Mootz implies that the O3 and O4 positions are OH^- sites in the Cs analog clathrate $\text{Cs}(\text{Me}_4\text{N})_2(\text{OH})_4 \cdot 14\text{H}_2\text{O}$, even though 16 O1–O1 distances $r_{\text{OO}} \approx 3.1$ Å according to his X-ray data; our results indicate that O1 positions are important hydroxide sites.

TMA also forms a low-temperature, semiclathrate $7.5\text{-}\alpha$ phase [1], which contains open polyhedral cages as a result of its proton deficiency, *i.e.* the water dynamics is presumably not fast enough to overcome the lack of hydrogen bonding along cage edges. In this case the $5^{12} 6^3$ P cage morphs into two improper polyhedra: a 16-hedron ‘Q’ with structure

³A Bjerrum D defect arises when two protons are between neighboring oxygen atoms.

Phase	Clathrate Phases	
	TMA ; Cs-TMA	TMA
Unit Cell	β (Hi T)	α (Low T)
Space Grp	Tetragonal	Triclinic
Cages:		
Small	$4^2 5^8$	$4^2(4)^1 5^5(5)^1$
Large	$5^{12} 6^3$	$(4)^1 5^9(5)^1 6^4(6)^1$ $4^2 5^6(5)^2 6^3(6)^2$
# Cages	4 Sm 8 Lg	2 Sm, 2 + 2 Lg
Cage Dia.	~ 3.5 Å $6.1 - 7$ Å	– –
Cage Vol.	100Å^3 300Å^3	80Å^3 300Å^3

Table 1: Unit cell structures for the high temperature β and low temperature α phases, along with the number and types of cages within each.

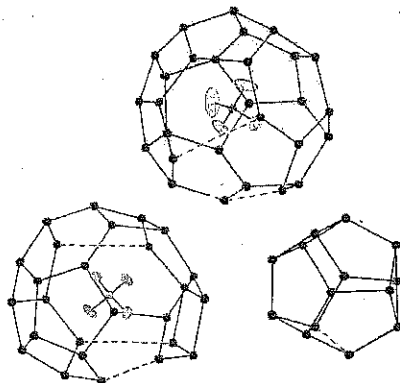


Figure 3: Semiclathrate (open) cages of the low-temperature 7.5- α form of the TMA clathrate [1]: $(4)^15^9(5)^16^4(6)^1$, $4^25^6(5)^26^3(6)^2$, and $4^2(4)^15^5(5)^1$ from top, counterclockwise.

$(4)^15^9(5)^16^4(6)^1$ and a 15-hedron 'R' with structure $4^25^6(5)^26^3(6)^2$, each containing a Me_4N^+ ion. The small 4^25^8 d cage distorts into an open nonahedron 's' with $4^2(4)^15^5(5)^1$; see Fig. 3 for α -phase cage schematics and Table 1. The resulting α -form has a unit cell formula of $2Q \cdot 2R \cdot 2s \cdot 4\text{OH}^- \cdot 30\text{H}_2\text{O}$, with 4 expanded interior cage edges corresponding to the eight, 3-coordinated OH^- ions, although Mootz does not give the associated non-bonded distances. Our structurally optimized cage structures display similarities to those shown in Fig. 3.

THEORY & SIMULATION METHODOLOGY

Ab initio structural optimizations and (short) molecular dynamics simulations of the TMA and Cs-TMA clathrates were carried out using the total energy density functional theory (DFT) [4, 5] methods implemented in the *Vienna Ab initio Simulations Package* (VASP) code [6, 7]. Exchange-correlation effects were taken into account using the generalized gradient approximation (GGA) functional PW91 [8, 9]. Core-valence electron interactions were described using the projector augmented-wave (PAW) method [10, 11] with an energy cutoff of 400 eV or 29.4 Rydbergs. Due to the large size of the unit cells ($a = 15.242 \text{ \AA}$, $c = 11.819 \text{ \AA}$), only the Γ point ($\mathbf{k} = 0$) was included in the Brillouin zone integrations. Periodic boundary conditions are utilized for all simulations.

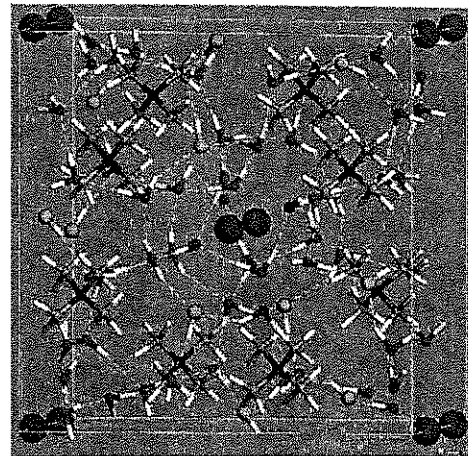


Figure 4: Initial Cs·TMA unit cell with the 12 OH^- shown in green, the Cs^+ in purple, the Me_4N^+ nitrogen in blue, and the oxygen in red.

Initialization

Initial positions for all but the protons in both TMA and Cs-TMA clathrate unit cells were taken from the X-ray diffraction data of Mootz and Stäben [2]. These clathrate lattices, like ice, are proton disordered, so generating water as well as methyl proton positions was done in several steps. Protein Data Bank [12] molecular structure files were used as templates to add the water and tetramethylammonium protons, which were then individually energy minimized with all heavy atoms fixed using the classical algorithms of NAMD [13]. All minimized molecules were then added to the unit cell and one final total energy minimization was conducted in NAMD ($\sim 2,000$ time steps) using CHARMM potentials, again allowing only the protons to relax. Finally, hydroxide sites had to be chosen. Since the O4 positions were 4-fold disordered, these 4 sites were chosen, along with 8 others taken randomly from the remaining water molecules for the OH^- sites in the Cs-TMA clathrate. This unit cell structure was then treated as the experimentally-determined 'X-ray' data and is shown in Fig. 4. The initial TMA unit cell was generated from this one simply by removing all Cs^+ ions from the small cages and returning 4 hydroxides to water molecules.

Thermalization

Since our *ab initio* structural optimizations of these large, hydrogen-bonded unit cells occur at 0 K, proton ordering effects must be treated carefully. Some recent work has been done to model proton order in isolated clathrate cages [14] as well as bulk gas hydrate lattices [15, 16]. Early evidence suggests that ionic clathrates may undergo partial proton ordering transitions at low temperature, much like ice Ih. Hence, in order to obtain more realistic proton lattice arrangements and improve statistical accuracy, short (*i.e.* costly) AIMD 'thermalization' runs were done to relax the water molecule orientations and to allow the protons to find lower energy (equilibrium) states. All atomic coordinates except for the protons were fixed in the *ab initio* geometry optimized TMA and Cs-TMA clathrates, and then the system was heated up to 5,000 K for a constant energy (NVE ensemble) *ab initio* molecular dynamics run. A 1 fs time step for integrating the equations of motion was used, and (quantum mechanical) electronic structure convergence was accepted when the energy difference between successive self-consistent iterations fell below 10^{-4} eV. With such a large unit cell, only ≈ 0.16 ps of real thermalization time was completed. Nevertheless, numerous water rotations and proton-transitions occurred in that time. A similar run was done for the X-ray refined TMA clathrate structure. Random coordinate frames from these thermalization runs were then re-optimized in order to determine their minimum energy structure (discussed below).

Structural optimizations

Geometry optimizations of all systems involved atomic coordinates only, with unit cell parameters fixed at the values determined from the X-ray data. Relaxation of the unit cell parameters may be important in determining possible phase transitions of the lattice, but are computationally much more costly and therefore are not done here. Several geometry optimizations were performed for each TMA and Cs-TMA system, the experimentally-determined X-ray structures (referred to as simply 'Opt' in the results) as well as a few of the randomly chosen thermalization frames (referred to as 'Reopt' in the results). Two reoptimization runs for the TMA lattice were done, Reopt A and B, while 4 reoptimization

Clathrate Energy Shifts

System	Total E (eV)	Reopt δE (eV)
TMA		
Opt X-ray	-1,686.25	0
Reopt A	-1,685.63	+0.620
Reopt B	-1,685.24	+1.01
Cs-TMA		
Opt X-ray	-1,681.92	0
Reopt C	-1,681.22	+0.701
Reopt D	-1,681.40	+0.520
Reopt E	-1,682.26	-0.340
Reopt F	-1,682.21	-0.290

Table 2: Total optimization and reoptimization energies for the TMA and Cs-TMA unit cells, along with the energy difference δE between the X-ray optimized and thermalized/reoptimized systems.

runs were completed for the Cs-TMA lattice, Reopt C through Reopt F. For these runs, VASP utilizes a *conjugate gradient* (CG) method of relaxing the ionic (core) positions to their lowest energy state after each electronic structure calculation is solved quantum mechanically. Once again electronic convergence was accepted when the total energy change between self-consistent CG iterations fell below 10^{-4} eV. Since the atoms do not carry any velocity here, the time step simply scales the magnitude of the steps taken in the 'downhill' direction.

RESULTS

The geometric optimization and reoptimization energies for the clathrates systems are shown in Table 2, along with the energy shift associated with first thermalizing the protons at 5,000 K and then reoptimizing one of the resulting configurations. As can be seen, neither of the two reoptimized, *i.e.* proton shuffled, TMA lattices is lower in energy than the originally optimized X-ray structure. For the Cs-TMA system, 2 of the 4 reoptimized structures are higher and 2 are lower in energy compared to the optimized X-ray configuration. It is important to note that these energies (shown in Table 2) are for the entire unit cell, such that energy spreads of ~ 1 eV between the various configurations in each system correspond to only about 0.07 kcal mol $^{-1}$, which happens to be the same order of magnitude as the 53° C melting temperature shift. Since the optimizations occur at 0 K, corresponding enthalpies

of formation can be calculated, but the large system size limits the methods available for determination of the zero-point vibrational energies (ZPVE).

Two central questions arise concerning the thermodynamic stability of these complementary ionic clathrates: (1) How are the hydroxide anions distributed within the host framework? and (2) What factors are responsible for the generous increase in melting temperature?

Filling the small cages with geometrically well-suited guests, *i.e.* the Cs^+ ions, should help stabilize the lattice simply through favorable van der Waals interactions, as is typically deduced for the sI and sII structures. The large monovalent Cs^+ ion, with a diameter of $d \approx 3.38 \text{ \AA}$, fits well within the small d cages, with experimentally determined distances $\langle r(\text{Cs} \cdots \text{O}) \rangle$ of 3.428 \AA and 3.527 \AA to the O1 and O2 oxygens. All of our optimized structures showed Cs^+ ions much closer to the cage walls, with $\langle r(\text{Cs} \cdots \text{O}) \rangle$ values of $\approx 3.527 \text{ \AA}$. Such distances correlate better with the van der Waals radii of oxygen rather than that of a water molecule, and most optimized water molecules were found to orient one or both of their O-H bonds tangent to the cage walls. Moreover, the ions, on average, tended to move closer to water oxygens in the cage walls than hydroxide oxygens, by about 0.15 \AA . The empty d cages in the TMA clathrates are slightly more distorted, with similarly defined diameters of 3.25 and 3.66 \AA .

Filling the 4^25^8 cages with Cs^+ guests, however, also entails an equal addition of hydroxide anions in the host framework, so more than simple cage occupancy effects must be considered in the stability of the clathrate. Equilibrium occupancy requirements for gas hydrate stability are usually determined via the theory of van der Waals and Platteeuw [17], a thermodynamic generalization of ideal localized adsorption, but calculations of the Langmuir adsorption constants, dependent upon accurate interaction potentials, for mixed and doubly occupied clathrates like those considered here, is a more complicated procedure [18]. Initial results, therefore, pertain to full (ideal) occupancy, but future work will include investigation of occupancy effects.

Hydroxide coordination

Perhaps the most interesting aspect of these ionic clathrates involves the incorporation of the hydrox-

ide anions into the water framework. Mootz *et al.* [1, 2] postulate hydroxide positions within the lattice loosely based upon the OH^- coordination deduced from their X-ray data of the tetrahydrate phase of TMA, along with the apparent stability of the $7.5\text{-}\beta$ phase despite its proton deficiency. Their X-ray data for the tetrahydrate shows a 4-fold coordinated hydroxide ion with the hydroxide proton H^* participating in a long (weak) hydrogen bond and much distorted tetrahedral angles. The long bond through the H^* proton, $(\text{OH}^*)^- \cdots \text{OH}_2$, showed a distance of $r_{\text{OO}} \approx 3.035 \text{ \AA}$, with the remaining three in the range $\approx 2.57\text{-}2.65 \text{ \AA}$. This long H^* -mediated hydrogen bond roughly correlates with the $\text{O3} \cdots \text{O3}$ and $\text{O3} \cdots \text{O4}$ distances of 3.19 and 3.25 \AA , as well as the 4-fold positional disorder of the O4 sites, leading Mootz to suggest that the hydroxides may be statistically distributed over these O3 and O4 positions.

The tetrahydrate OH^- coordination distances found by Mootz are supported by more recent work, such as the spectroscopic studies of $\text{OH}^- \cdot (\text{H}_2\text{O})_n$ clusters by Robertson *et al.* [19] and the theoretical OH^- solvation studies of Asthagiri *et al.* [20, 21]. The latter statistical mechanical and *ab initio* research found that the most stable (lowest hydration free energy) state of the $\text{OH}^-(\text{aq})$ anion is $\text{HO} \cdot [\text{H}_2\text{O}]_3^-$, *i.e.* 3 hydrogen bonded neighbors in the first solvation shell. Qualitatively, the hydroxide hydrogen H^* is less positively charged than is typical for water protons. Thus the fourth water ligand prefers to crowd among the other three on the oxygen side of the hydroxide anion; the aqueous hydroxide proton H^* tends not to participate in hydro-

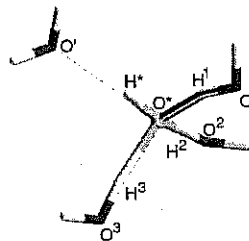


Figure 5: Coordination nomenclature for the (green) hydroxide anion $\text{O}^* - \text{H}^*$. Here O^* is the (H^*) proton acceptor, while O^1 , O^2 , and O^3 are proton donors to the hydroxide.

Hydroxide Coordination

System			TMA	
[Å] (Std. Dev.)	Expt. [†]	(Reopt.) [§]		
O*...O'	3.42 (0.260)	3.43 (0.291)		
O*...O ¹	2.54 (0.049)	2.55 (0.038)		
O*...O ²	2.60 (0.051)	2.63 (0.046)		
O*...O ³	2.70 (0.058)	2.69 (0.045)		
System			Cs·TMA	
[Å] (Std. Dev.)	Expt. [†]	(Reopt.) [§]		
O*...O'	3.21 (0.294)	3.19 (0.258)		
O*...O ¹	2.55 (0.0551)	2.54 (0.050)		
O*...O ²	2.62 (0.033)	2.62 (0.039)		
O*...O ³	2.67 (0.037)	2.68 (0.046)		

[†] Optimized X-ray data with artificially positioned protons

[§] Average of 2 (TMA) and 4 (Cs·TMA) reoptimized structures

Table 3: Average O*...Oⁱ coordination distances (r_{OO}) from the hydroxide oxygen O* to the coordinating oxygen O', O¹, O², and O³, as shown in Fig. 5.

gen bonding.

We find similar asymmetrical hydroxide coordination in all of our minimum energy, optimized structures consistent with a weakly bonded or free H⁺ proton. Figure 5 shows a general bonding scheme for the (green) hydroxide in our studies. A 3-fold coordinate vertex in the clathrate lattice poses definite stability concerns, as a reduction in the static number of hydrogen bonds along cage edges (below 136 in this case) would suggest a less stable lattice and a lower melting temperature. Table 3 displays the relevant hydroxide coordination distances O*...Oⁱ defined in Fig. 5. There 'experimental' values correspond to the optimized X-ray data with only classically-minimized proton positions. As found by Asthagiri *et al.*, the O*...O' r_{OO} distance is the longest of the four, with the other three being distributed over a range of values instead of being equal, the shortest⁴ (≈ 2.5 Å) classified as a strong hydrogen bond. The central feature to note is that all coordination distances O*...Oⁱ, where $i \in \{1, 2, 3\}$, are essentially equal with small distributions: experimental and reoptimized values for a given clathrate as well as those for both TMA and Cs·TMA clathrates. The coordination distance through the hydroxide proton O*...O', however, decreases by about ~ 0.2 Å for the cesium-based ana-

⁴Here always O*...O¹ because of the algorithm used.

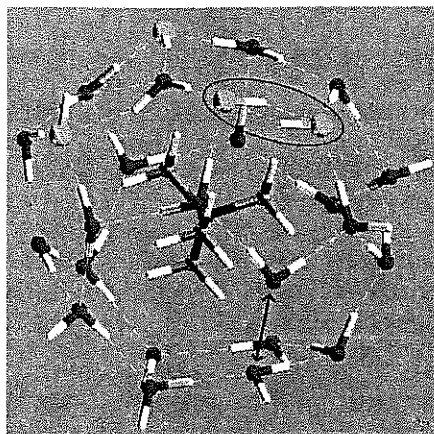


Figure 6: Large (P) cage from a reoptimized TMA lattice with a Bjerrum D defect shown (circled in brown) between neighboring hydroxides. An open hexagonal and pentagonal face is also shown.

log. The TMA O*...O' distance of 3.4 Å would be quite long even for a weak hydrogen bond. The addition of 4 Cs⁺ and 4 additional OH⁻ ions seems to shorten this long r_{OO} distance, while leaving the other distances unchanged.

This difference in O*...O' coordination alone does appear to make some characteristic differences in the TMA and Cs·TMA cages. Shown in Figs. 6 and 7 are several cages from the TMA and Cs·TMA clathrates, respectively. The hydroxide protons H⁺ in the TMA clathrates appear to be more directionally disordered, *i.e.* not directed along cage edges, and some Bjerrum D defects appear (see Fig. 6). In contrast, the hydroxide orientations in the Cs·TMA clathrate appear to be much more aligned along cage edges, as shown in Fig. 5. In one case, however, a hydroxide proton appears to be oriented inside a large cage (see Fig. 7). It should be noted, however, that the number of simulations is rather small, limiting the statistics. Another interesting note is that all O*...Oⁱ distances seem to increase up to ~ 0.1 Å as the ionic radius of the small guest decreases from Cs down to Li.⁵

⁵Simulation data not shown.

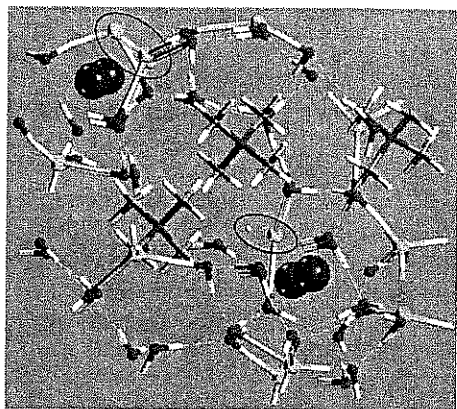


Figure 7: Several large and small cages (c axis \perp to paper) from a reoptimized Cs·TMA lattice. Hydroxide anions (green) occupy O2 positions (square faces) of the small cages (upper brown circle). One hydroxide proton H^* , shown 'unbonded' 0.972 \AA away from its oxygen O^* (central brown circle), is oriented inside a large cage.

Hydroxide distribution

The static distribution of hydroxide anions within the unit cell shows some disagreement with that inferred from the X-ray data. As Table 4 indicates, roughly half of the water molecules within the unit cell have hydroxide anions as neighbors, the higher values associated with the Cs·TMA system simply a result of the fact that it contains 12 instead of just 8 hydroxide ions. Moreover, all reoptimized structures contain one OH^- pair, although these pairs are not (in the limited statistics given) always located at the same crystallographic positions. Contrary to the assumptions of Mootz, the hydroxide sites do not seem to be limited to the O3 and O4 positions. The initial configuration of the hydroxides (Fig. 4) included all four O4 positions, one O3, and seven O1 sites. Of these O4 positions, only one remained a hydroxide site after optimization, which remained in all TMA clathrate lattices, but is in only 2 of the 5 Cs·TMA optimized lattices. A majority of the hydroxides settle in O1 positions, with both O2 and O3 a close second. There does seem to be some prevalence for hydroxide ions to settle into specific crystallographic sites, but the limited statistics has to temper any firm conclusions. The dominant lack of any hydroxides at the O4 positions, as well as the re-

$n =$	% H_2O with n OH^- neighbors				Number of OH^- pairs
	0	1	2	3	
TMA					
Opt X-ray	55	40	5	–	0
Reopt A	52	42	4	2	1
Reopt B	58	33	7	2	2
Cs·TMA					
Opt X-ray	28	54	18	–	0
Reopt C	34	50	16	–	1
Reopt D	29	55	12	4	0
Reopt E	34	50	16	–	1
Reopt F	34	50	16	–	1

Table 4: Distribution of OH^- throughout the unit cell: % of water molecules with 0, 1, 2, or 3 hydroxide anions in the first coordination shell. Far right column: number of nearest-neighbor hydroxide pairs.

currence of a few other crystallographically distinct positions, however, is suggestive of possible hydroxide ordering within the unit cell.

Regardless of where the hydroxides are initially positioned, proton transfers do occur during the *ab initio* structural optimizations. Table 5 shows the total number of proton transitions that occurred during a given optimization run. Not all transitions listed, however, occurred between nearest neighbors. This is simply an artifact of the hydroxide identification algorithm and the unphysical proton configura-

Proton Transitions

System	# Trans.	$\langle r_{O^*O} \rangle$ [\AA]
TMA		
Opt X-ray	14	2.43
Reopt A	6	2.44
Reopt B	6	2.43
Cs·TMA		
Opt X-ray	21	2.44
Reopt C	4	2.44
Reopt D	5	2.44
Reopt E	9	2.44
Reopt F	8	2.45

[§] Average may not include all transitions.

Table 5: Total number of proton transitions during geometric optimizations and the average $O^* \cdots O$ distance $\langle r_{O^*O} \rangle$ for those transitions that occur between neighboring hydroxide and water oxygens.

Long O...O Distances

System	Number of $r_{OO} > 3.25 \text{ \AA}$	% incident upon an OH^-
TMA[†]		
Opt	16	37.50
Reopt A	16	31.25
Reopt B	17	35.29
Cs-TMA[§]		
Opt	19	36.84
Reopt C	16	31.25
Reopt D	18	33.33
Reopt E	18	33.33
Reopt F	16	37.50

[†] Eight hydroxides in the unit cell.

[§] Twelve hydroxides in the unit cell.

Table 6: Approximate number of O...O distances $r_{OO} > 3.25 \text{ \AA}$, and percentage of those r_{OO} that are incident upon an hydroxide anion.

tions encountered in the initial or relaxing systems.⁶ For the thermalized and reoptimized systems, however, ≈ 75 –100% of all proton transitions occurred between nearest neighbors as $\text{HO-H}\cdots(\text{*OH})^- \rightarrow (\text{HO*})^- \cdots \text{H-OH}$. The short $\text{O}^* \cdots \text{O}'$ distances involved, $\langle r_{O'O} \rangle \approx 2.44 \text{ \AA}$, are consistent with a zero barrier transition [14, 22]. As evident from the table, thermalization creates more stable water orientations but not necessarily lower energy ones (compare with Table 2).

Clathrates or Semiclathrates?

The seemingly large number of long O...O distances ($\geq 3.25 \text{ \AA}$) within the host lattice, many between water molecules, calls into question whether or not these cages edges can be hydrogen bonded. The (0 K) ground state polyhedral cages certainly appear to be open or 'improper' based upon static distances alone, and show similar traits to those semiclathrate cages displayed by the low temperature α phase of the TMA clathrate (see Fig. 3). Mootz *et al.* attributed the longest r_{OO} distances in the unit cell to the long hydroxide coordination

⁶The 5,000 K thermalization runs created some high-energy proton configurations, e.g. $\text{H}_2\text{O}\cdots\text{H}\cdots\text{OH}$, which were temporarily counted as hydroxide ions because of the symmetric position of the mediating proton. These structures always relaxed to neutral water molecules, but did lead to artificially large r_{OO} proton transition distances well beyond nearest neighbors.

Optimization Shifts

Atom	$B^{\text{exp}} (\text{\AA}^2)$	$\delta^{\text{exp}} (\text{\AA})$	TMA [†] $\langle \Delta r \rangle (\text{\AA})$
O1	1.46	0.136	0.358
O2	1.44	0.135	0.449
O3	3.16	0.200	0.350
O4	5.32	0.260	0.444
N	1.46	0.136	0.223
Atom	$B^{\text{exp}} (\text{\AA}^2)$	$\delta^{\text{exp}} (\text{\AA})$	Cs-TMA [‡] $\langle \Delta r \rangle (\text{\AA})$
Cs	1.33	0.130	0.351
O1	1.76	0.149	0.349
O2	1.16	0.121	0.325
O3	1.97	0.158	0.282
O4	1.89	0.155	0.197
N	1.54	0.140	0.200

[†] TMA reoptimization B

[‡] Cs-TMA reoptimization D

Table 7: Experimental isotropic thermal parameters B (-50°C) and their equivalent vibrational amplitudes δ , compared to some average positional shifts Δr arising from structural optimizations.

configurations $\text{O}^* \cdots \text{O}'$, thus placing all OH^- at the O3 and O4 positions. Our results indicate that, not only are the hydroxide anions more distributed throughout the crystallographically distinct O'_i sites than suggested by Mootz, but that the $\text{O}^* \cdots \text{O}'$ distances are not the only 'long' r_{OO} distances in the unit cell. As Table 6 shows, a sizeable fraction of the 136 cage edges in the unit cell, from ~ 12 –14%, exceed 3.25 \AA , the longest distance found in X-ray studies. We found a spectrum of distances above 3.25 \AA , all the way up to $\approx 4.0 \text{ \AA}$ —although a few of those largest r_{OO} distances correspond to very small O–O angles, *i.e.* to next-nearest neighbors located within the same cage.⁷ Several 'long' r_{OO} distances are evident in the cages shown in Figs. 6 and 7. Those in the former look quite similar to the open (6)¹ and (5)¹ faces in the 7.5- α phase of the TMA clathrate (see Fig. 3).

As a further indication that the original configuration of the TMA and Cs-TMA clathrates determined by Mootz *et al.* (at -50°C) may not be statically stable, we compared the equivalent vibrational am-

⁷O–O angles less than the tetrahedral 109.5° can shift typical next-nearest neighbor distances in from 4.5 \AA to $\sim 4.0 \text{ \AA}$, while disorder may shift nearest neighbors further away.

plitudes δ from the X-ray data, derived from the isotropic thermal parameters $B = 8\pi^2\langle u^2 \rangle$, with the averaged positional shifts Δr associated with the *ab initio* geometric optimizations, tabulated in Table 7. Nearly all crystallographically distinct atoms move well beyond their vibrational amplitudes during the optimization procedure at 0 K, apart from the nitrogen atoms in the TMA⁺ ions. This suggests that the high temperature 7.5- β phase of the TMA clathrate, along with its alkali analog Cs-TMA, may only be dynamically stable. Clearly more work is needed to determine whether a low temperature phase transition occurs in these complementary systems (*e.g.* β to α type), or if this apparent semiclathrate cage structure for both TMA and Cs-TMA systems can be effectively closed via alkali ion induced proton transport mechanisms. Many studies of low temperature proton ordering transitions in normal ice exist, but very little theoretical work has yet been done for such ordering in ionic clathrate hydrates [15, 16]. Given the ideal tetrahedral coordination of these gas hydrates, we hope to modify current statistical mechanical-based quasichemical theory, coupled with *ab initio* methods, to approximate proton ordering effects within these ionic systems in the near future.

REFERENCES

- [1] D. Mootz and R. Seidel, *J. Incl. Phenom. Mol. Recog. Chem.* **8**, 139 (1990).
- [2] D. Mootz and D. Stäben, *J. Am. Chem. Soc.* **116**, 4141 (1994).
- [3] N. Bjerrum, *Science* **115**, 385 (1952).
- [4] P. Hohenberg and W. Kohn, *Phys. Rev.* **136**, 864 (1964).
- [5] W. Kohn and L. J. Sham, *Phys. Rev. A* **140**, 1133 (1965).
- [6] G. Kresse and J. Hafner, *Phys. Rev. B* **47**, RC558 (1993).
- [7] G. Kresse and J. Furthmüller, *Phys. Rev. B* **54**, 11169 (1996).
- [8] Y. Wang and J. P. Perdew, *Phys. Rev. B* **44**, 298 (1991).
- [9] J. P. Perdew et al., *Phys. Rev. B* **46**, 6671 (1992).
- [10] P. E. Blöchl, *Phys. Rev. B* **50**, 17953 (1994).
- [11] G. Kresse and J. Joubert, *Phys. Rev. B* **59**, 1758 (1999).
- [12] H. M. Berman et al., *Nucleic Acids Research* **28**, 235 (2000), See <http://www.pdb.org>.
- [13] L. Kal et al., *J. Comp. Phys.* **151**, 283 (1999).
- [14] J. Kuo, C. V. Ciobanu, L. Ojamäe, I. Shavitt, and S. J. Singer, *J. Chem. Phys.* **118**, 3583 (2003).
- [15] M. V. Kirov, *J. Struct. Chem.* **43**, 266 (2002).
- [16] M. V. Kirov, *J. Struct. Chem.* **43**, 980 (2002).
- [17] J. H. van der Waals and J. C. Platteeuw, *Adv. Chem. Phys.* **2**, 1 (1959).
- [18] B. J. Anderson, J. W. Tester, and B. L. Trout, *J. Phys. Chem. B* **108**, 18705 (2004).
- [19] W. H. Robertson, E. G. Diken, E. A. Price, J. Shin, and M. A. Johnson, *Science* **299**, 1367 (2003).
- [20] D. Asthagiri, L. R. Pratt, J. D. Kress, and M. A. Gomez, *Chem. Phys. Lett.* **380**, 530 (2003).
- [21] D. Asthagiri, L. R. Pratt, J. D. Kress, and M. A. Gomez, *PNAS* **101**, 7229 (2004).
- [22] D. Borgis, G. Tarjus, and H. Azzouz, *J. Chem. Phys.* **97**, 1390 (1992).